Engineering Software Research & Development, Inc.
111 West Port Plaza, Suite 825
St. Louis, MO 63146

# Final Technical Report

## STTR Grant No: FA9550-05-C-0128

## Software for the Design and Certification of Unitized Airframe Components

**Performing Organization**: Engineering Software Research and Development, Inc
**Principal Investigator:** Dr. Ricardo Actis, 314-744-5021 ext. 15
**Academic Institution:** Washington University in St. Louis
**Principal Investigator for the Academic Institution:** Prof. Barna Szabó, 314-935-6352
**Reporting Period:** 08/01/05 – 02/01/06
**Date of report:** 02/23/06

# Abstract

This report presents the results of the investigation of two important subjects associated with the design and certification in unitized airframe components. The first subject is related to the effects of residual stresses on the structural stability of thin unitized components machined from aluminum plates, in particular 7050-T74 and 7050-T7451 plates. The findings indicate that residual stresses introduced in a plate during the rolling operation (bulk stresses) and residual stresses introduced into a part machined from the plate during high speed machining should be included as a modeling consideration when designing thin unitized components. The second subject is related to the computation of strain energy release rate in damaged laminate composite materials. Typical failure in the presence of an initial defect, such as delamination, appears under a mixed mode loading, therefore it is essential to have an efficient algorithm for the computation of the strain energy release associated with each loading mode for the construction a mixed mode failure criterion for the determination of residual strength of unitized components made of composite materials. The Virtual Crack Closure Technique (VCCT) was considered during the Phase I project. It was found that typical numerical implementations of the VCCT utilizing the h-version of the finite element method (FEM) are unreliable because the results are mesh-dependent. A modification of the method was investigated, involving a combination of numerical and analytical computations, which is well suited for its implementation with the p-version of the Finite Element Method.

# Introduction

Increasing emphasis on affordability of military systems has led to a number of advances in airframe design and production. Unitized airframe structural components are replacing sheet metal built-up components to reduce part count and assembly cycle times and costs. The development of high speed machining (HSM) techniques has made it possible to fabricate thin lightweight structures that provide improved performance at lower costs. There is a need for advanced numerical methods for the solution of problems associated with the manufacturing and certification of unitized airframe components. The goals are to support (a) damage tolerant designs, (b) establishment of criteria for inspection intervals, (c) planning the fabrication processes so that the incidence of re-working and scrapping of partially or fully manufactured parts is substantially reduced, and (d) evaluation of options for reworking and clear criteria for decisions whether to certify or reject an as-manufactured part. This is expected to result in

# REPORT DOCUMENTATION PAGE

*Form Approved*
*OMB No. 0704-0188*



| **1. REPORT DATE** *(DD-MM-YYYY)* | **2. REPORT TYPE** | **3. DATES COVERED** *(From - To)* |
|---|---|---|
| 02-23-2006 | Final Technical Report | Aug 1, 2005 – Feb 1, 2006 |

**4. TITLE AND SUBTITLE**

Software for the Design and Certification of Unitized Airframe Components

**5a. CONTRACT NUMBER**

**5b. GRANT NUMBER**
FA9550-05-C-0128

**5c. PROGRAM ELEMENT NUMBER**

**6. AUTHOR(S)**
Dr. Ricardo Actis

**5d. PROJECT NUMBER**

**5e. TASK NUMBER**

**5f. WORK UNIT NUMBER**

**7. PERFORMING ORGANIZATION NAME(S) AND ADDRESS(ES)**

Engineering Software Research
& Development, Inc.
111 West Port Plaza,
Suite 825
St. Louis, MO 63146

**8. PERFORMING ORGANIZATION REPORT NUMBER**

**9. SPONSORING / MONITORING AGENCY NAME(S) AND ADDRESS(ES)**
Air Force Office of
Scientific Research (AFOSR)
Attn: Dr. Fariba Fahroo
875 North Randolph Street,
Arlington, VA 22203

**10. SPONSOR/MONITOR'S ACRONYM(S)**
AFOSR

**11. SPONSOR/MONITOR'S REPORT NUMBER(S)**
AFRL-SR-AR-TR-06-0474

**12. DISTRIBUTION / AVAILABILITY STATEMENT**

Approved for public release; distribution is unlimited.

**13. SUPPLEMENTARY NOTES**
N/A

**14. ABSTRACT**

This report presents the results of the investigation of two important subjects associated with the design and certification in unitized airframe components. The first subject is related to the effects of residual stresses on the structural stability of thin unitized components machined from aluminum plates, in particular 7050-T74 and 7050-T7451 plates. The findings indicate that residual stresses introduced into a part machined from the plate during high speed machining should be included as a modeling consideration when designing thin unitized components.

**15. SUBJECT TERMS**

| **16. SECURITY CLASSIFICATION OF:** | | | **17. LIMITATION OF ABSTRACT** | **18. NUMBER OF PAGES** | **19a. NAME OF RESPONSIBLE PERSON** |
|---|---|---|---|---|---|
| **a. REPORT** | **b. ABSTRACT** | **c. THIS PAGE** | | | Prof. Yanzhao Cao |
| Unclassified | Unclassified | Unclassified | | 32 | **19b. TELEPHONE NUMBER** *(include area code)* (314) 744-5021 |

**Standard Form 298 (Rev. 8-98)**
**Prescribed by ANSI Std. Z39.18**

substantial affordability improvements for aircraft and spacecraft structures as well as increased reliability.

Most aluminum and many titanium aircraft components are fabricated by milling out 90 to 95 percent of the material from plate stock. Typical parts consist of large numbers of open pockets with thin bottoms (webs), enclosed by thin walls (ribs) perpendicular to the webs. The webs and ribs are connected by filleted transition regions. The problem class is sufficiently large, important and complex to warrant development of specialized software for analysis and design.

It is necessary to have the capability to verify and validate the mathematical models that serve as a basis for engineering decisions. Parametric modeling capabilities based on the hierarchic concept of models, that allow dimensional reduction where appropriate, and account for non-linearities when necessary, provide the mathematical and technological basis for reliable numerical simulation procedures.

The problem of buckling (oil canning) was observed in machining experiments conducted at the Machining Development Laboratory of the Boeing Phantom Works, St. Louis, Missouri. It was noted that thin-walled test articled buckled upon removal from the fixtures. The results of preliminary investigations suggest that the machining-induced residual stresses are the primary cause for buckling.

The Phase I effort focused on the conceptual basis of an algorithmic structure designed to meet the objectives indicated above and development of an implementation plan. ESRD consulted with AFRL Materials and Manufacturing Directorate and aerospace OEMs (The Boeing Company in St. Louis, Missouri and Lockheed Martin Aeronautics in Marietta, Georgia) in the formulation and prioritization of the technical objectives. During these consultations it became apparent that a useful tool for the analysis and design of unitized structural component should also include a capability to determine the residual strength of damaged structures made of composite materials. The strain energy release rate was identified as the key parameter that characterizes the residual strength of unitized structures made of laminate composites.

Since composite materials generally exhibit a coupling between load and deformation modes (i.e., a symmetric loading may lead to a deformation that is not purely symmetric) due to lack of symmetry in material properties, Mode I, Mode II and Mode III loading are expected to be present in most cases when fracture mechanics parameters for composite materials have to be determined. The most promising characterizing parameters for the onset of propagation in composites is the energy release rate associated with each mode of deformation. During the Phase I project the virtual crack closure technique (VCCT) within the framework of the p-version of the finite element method was investigated as the algorithm for the computation of the energy release rate for Mode I and Mode II in composite materials for 2-dimensional problems.

The following tasks were performed during the Phase I investigation:

1. Preliminary investigation of the effects of residual stresses caused by (a) the manufacturing process of 7050-T74 and 7050-T7451 aluminum plate stock and (b) mechanical milling on the structural stability of unitized metallic airframe components. Machining-induced stresses result from the interaction between the work piece and the cutting tool. These stresses are estimated to be of the order of 150 MPa, within a boundary layer of approximately 0.3 mm. The stresses decay rapidly outside of the boundary layer. This poses a challenging computational problem, because elements near the boundary need to have very large aspect ratios. During the Phase I investigation the available residual stress profiles were utilized to determine the sensitivity of the classical buckling strength to the magnitude and distribution of residual stresses.
2. An algorithm for the determination of the buckling strength of unitized metallic airframe components that accounts for the effects of residual stresses was developed. In view of the fact that the loading data, material properties and, to a lesser extent, the geometric properties are stochastic, the algorithm needs to be enhanced to allow rapid evaluation of alternative designs, support parametric optimization procedures and Monte Carlo simulations.
3. Preliminary investigation of the proper algorithm for the computation of energy release rates for defects, such as delamination in unitized structures made of composite materials.

ESRD's software product StressCheck was utilized during the Phase I investigation.

# Residual stresses

## *Effect of residual stresses on pre-load buckling*

Consider the box like test specimen machined from an aluminum plate[1] (Figure 1). Prior to removing the specimen from the machining fixture no signs of buckling were present, but after removing the specimen from the fixture it buckled in a typical 'oil can' mode.

[1] Provided by The Boeing Company, Phantom Works, St. Louis MO.

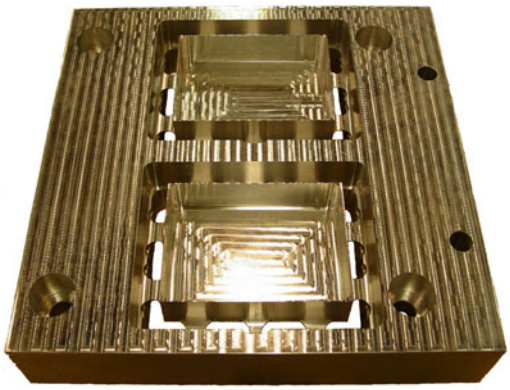

**Figure 1: Test specimen on fixture frame.**

Since buckling is observed after removing the specimen from the fixture, residual stresses alone can be considered to be the source of the instability (therefore the use of the term pre-load buckling). Residual stresses can be classified into two types, the first are the residual stresses caused by the metal forming process, called bulk or material stresses; the second are the residual stresses introduced during the machining process (i.e., machining-induced residual stresses). To determine whether the bulk stresses, the machining induced stresses or a combination of both is causing the specimen to buckle, two sets of numerical studies were performed using a finite element representation of similar dimensions as the test specimen (Figure 2). The effects of one type of residual stresses only were considered for each set.

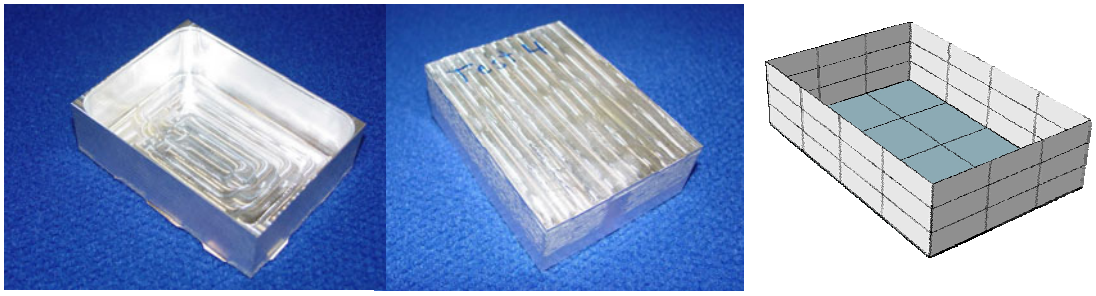

**Figure 2: Test specimen and finite element mesh.**

For the numerical simulation, the fillets between the web and the flanges were omitted from the model. This simplification is acceptable for buckling analysis since the presence of these geometric details do not significantly affect the results.

## Effect of bulk residual stresses on pre-load buckling

The model shown in Figure 2 was loaded with bulk residual stresses typical of those in 76 mm thick, 7050-T74 (heat treated only) and 7050-T7451 (heat treated and stretched) aluminum plates

shown in Figure 3 ([1], [2]). An eigen-value buckling analysis was performed in order to obtain the critical buckling load and mode shape, for different locations of the test specimen through the thickness of the plate as indicated schematically in Figure 4. (The parameter *ex* is a measure of the eccentricity of the box with respect to the mid-plane of the plate).

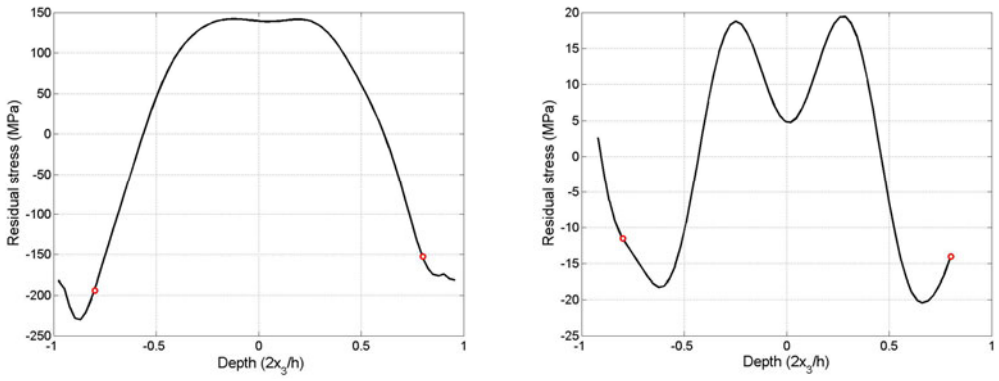


**a)** **b)**

**Figure 3: Typical Residual stresses in a 76 mm thick aluminum plate: a) 7050-T74 b) 7050-T7451.**

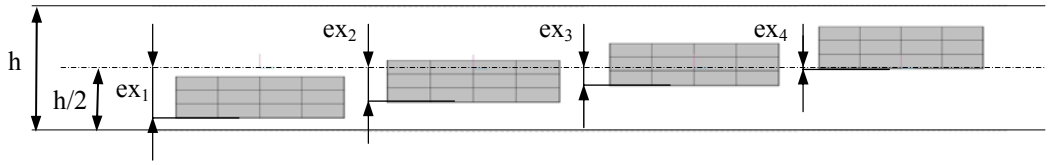


**Figure 4: Location of the box with respect to the plate where it is machined from.**

The study was restricted so that the box was contained within the interval $-0.8 \le 2x_3/h \le 0.8$ because there is no information of residual stresses outside this interval (indicated by dots in Figure 3) and extrapolation would not be reliable. The coordinate $x_3$ is in the thickness direction, and $h$=76 mm.

The computed load factors and typical mode shapes are shown in Table 1 and Figure 5 respectively. The load factor is the multiplying factor that must be applied to the residual stresses to produce buckling. If a load factor is greater than 1.0, then the specimen will not buckle under the given residual stress distribution.

**Table 1: Buckling Load Factor for boxes machined from 7050-T74 and 7050-T7451 aluminum plates.**

| Location | ex [mm] | Load Factor 7050-T74 | Load Factor 7050-T7451 |
|---|---|---|---|
| 1 | 30.32 | 3.39 | 6.12 |
| 2 | 21.51 | 4.29 | 7.28 |
| 3 | 12.7 | 15.78 | 11.78 |
| 4 | 3.89 | 6.53 | 14.64 |
| 5 | -4.92 | 3.48 | 5.59 |

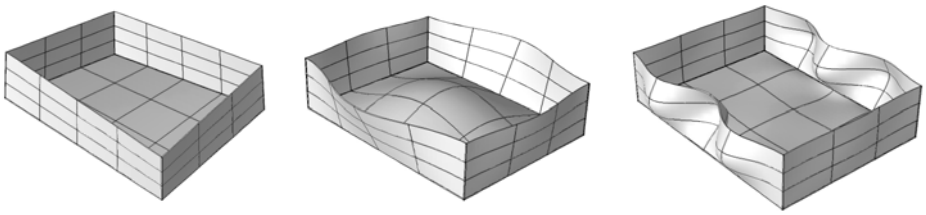

**Figure 5: Typical mode shapes (1st mode) for pre-load buckling under bulk stresses. Far left for all values of ex for 7050-T74. Center for ex=30.32, and right for ex=3.89 for 7050-T7451.**

The residual stresses were incorporated into the model shown in Figure 2 by specifying formula-based coefficients of thermal expansion as described in [1]. The dimensions of the model were selected such that they are representative of the specimens shown in Figures 1 and 2 (76.2x101.62x25.4 $mm^3$, with 3.81 mm thick walls).

The investigation showed that the bulk residual stresses are insufficient (and very far) from causing the specimen to buckle and that, in some cases, the associated buckling mode was very different from the observed 'oil can' mode in the test specimens. It was therefore concluded that the bulk stresses (from 7050-T74 or 7050-T7451 aluminum plates) cannot cause the buckling observed in the test specimens. It follows that machining-induced residual stresses are the probable cause for buckling of thin parts machined from metal plates. This is discussed in the following section.

## Effect of machining-induced residual stresses on pre-load buckling

In the study described in the previous section it was determined that the bulk stresses present in 7050-T74 or 7050-T7451 aluminum plates cannot be the sole cause of buckling after machining. In this section, results are presented for the model loaded with typical machining-induced stress profiles, neglecting bulk stresses.

The machining-induced residual stress profiles used in this study were obtained from experiments performed on specimens machined from 7050-T7451 aluminum plates with similar tools (end mill) as those used for analyzing the test specimens shown in Figures 1 and 2. Figure 6 shows a schematic of the test specimens used for computing the machining-induced stresses (see [2], [3], [4] for details). The set of specimens consisted of two groups, one corresponding to specimens machined with the side of the tool (rib specimens), and the other corresponding to specimens machined with the head of the tool (web specimens), as shown in Figure 7. This distinction was made not only because residual stresses induced by machining the material with the head or side of the tool were expected to be different, but also because most thin unitized components can be considered as a collection of ribs and webs.

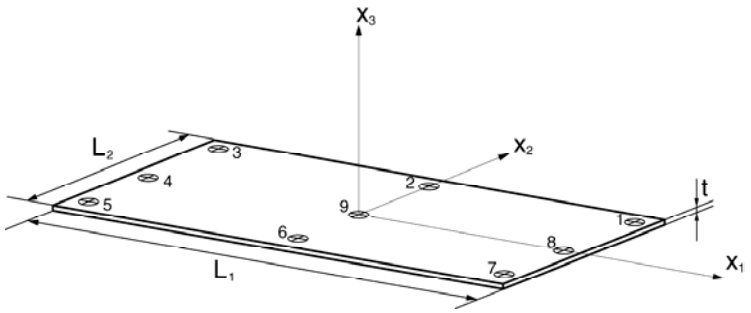


**Figure 6: Test specimen description used in the computation of machining-induced residual stresses.**

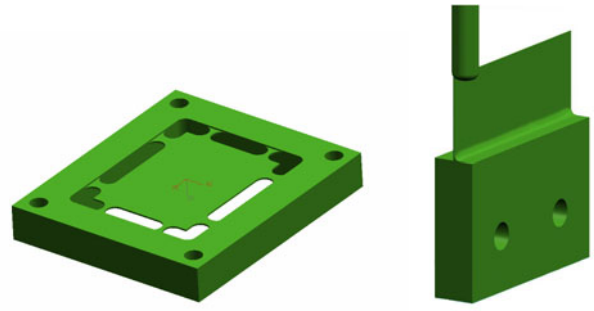

**a)** **b)**

**Figure 7: Test specimens: (a) Web specimen; (b) Rib specimen.**

Since experimental information of the residual stress profiles around corners of fillets is unavailable these are not considered in this investigation. It is expected however, given the rigidity of these components, that this simplifying assumption will not significantly affect the results. Figures 8 and 9 show the residual stress profiles used in this study.

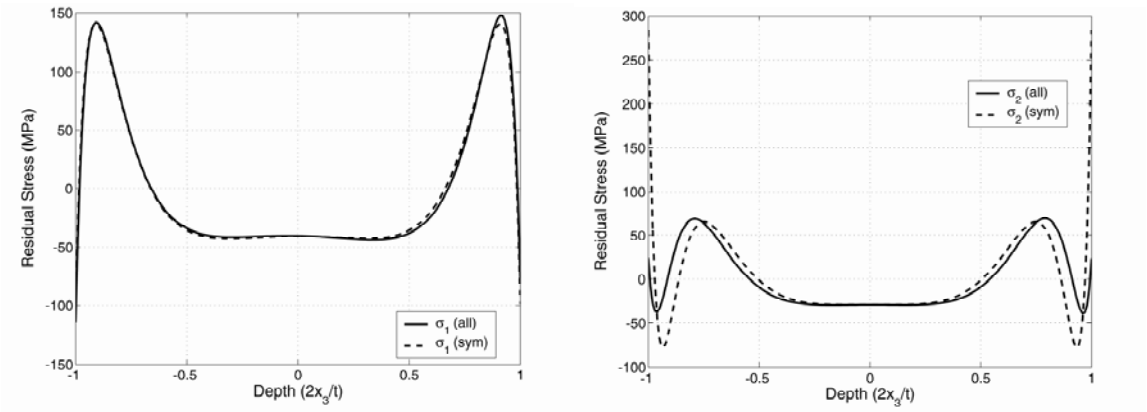


**Figure 8: Residual stress profiles for a thin rib ($\sigma_x$ and $\sigma_y$ respectively)**

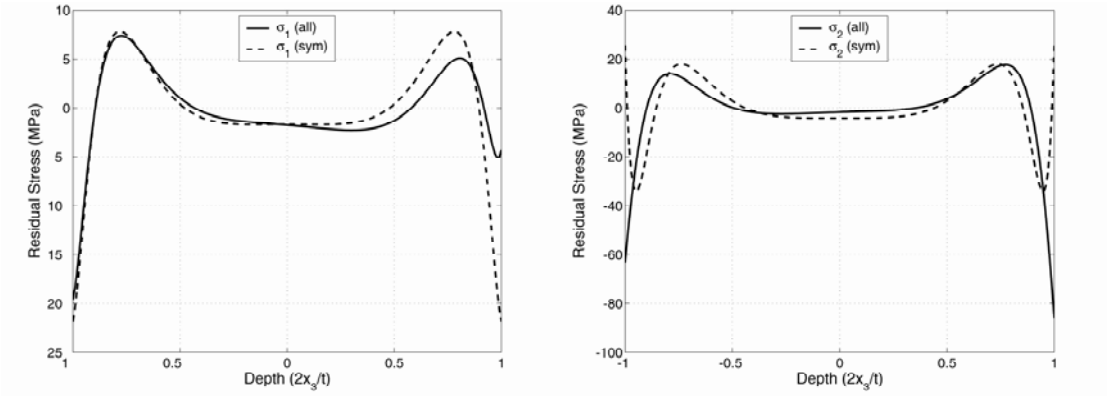


**Figure 9: Residual stress profiles for a thin web ($\sigma_x$ and $\sigma_y$ respectively)**

Machining-induced stresses resulting from the interaction between the work piece and the cutting tool are of the order of 150 MPa, within a boundary layer of approximately 0.3 mm. The stresses decay rapidly outside of the boundary layer. This poses a challenging computational problem, because elements near the boundary need to have very large aspect ratios. This difficulty is easily overcome by the p-version of the finite element method [8]. In order to provide an accurate approximation, the finite element mesh was designed with four elements through the thickness of the specimen as shown in Figure 10. The quality of the solution was ascertained by running 8 linear solutions from p=1 to 8, and checking the convergence of the linear solution before performing the buckling analysis.

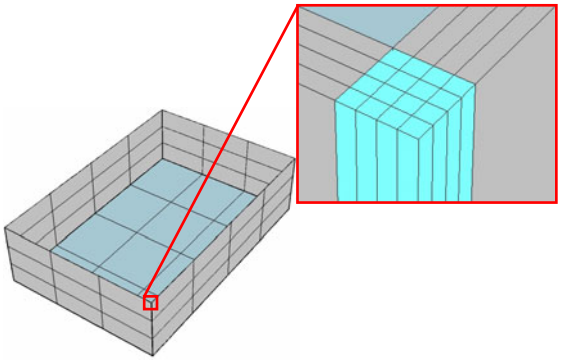

**Figure 10: Mesh layout and detail.**

The first buckling mode is shown in Figure 11a, where the computed load factor (Ld. Fct.) was 2.34e-01. It follows that a specimen machined with the same tool that produced the residual stress profiles used in this study will buckle once removed from the fixture. The second buckling mode, shown in Figure 11b, is the typical 'oil can' mode. The load factor was computed as 1.433, which is very close to 1. Given the fact that the machining-induced stresses are rough estimates only, it is probable that this mode will occur also.

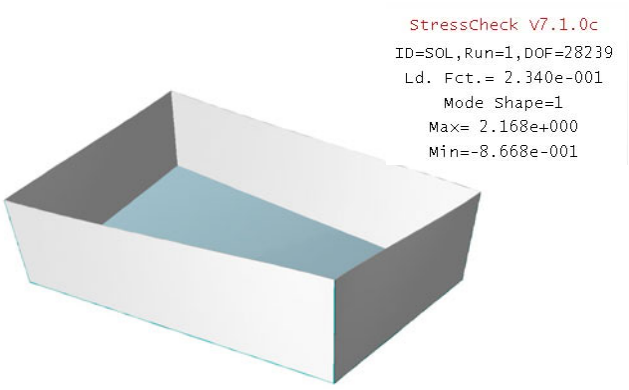


**Figure 11a: First buckling mode and load factor.**

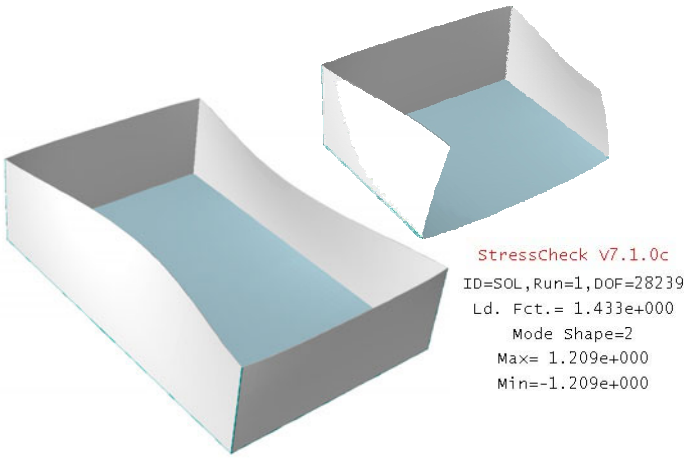


**Figure 11b: Second buckling mode and load factor.**

At this time no reliable methods exist for the determination and mathematical representation of machining-induced stresses. Pre-load buckling in parts machined from aluminum metal plates may be prevented by removal of the layer of material affected by the machining process (denoted as plastic layer) using a process such as chemical milling (which is supposed to introduce no residual stresses) as described in [2]. By removing the plastic layer, the specimen will be affected mainly by bulk stresses, for which it is expected that pre-load buckling will be prevented.

## *Effect of bulk residual stress on strength buckling*

In most analysis performed using the theory of elasticity, initial stresses are neglected, the main reason being the lack of available information about their distribution. This is a reasonable assumption when the part to be analyzed has thick walls. In the case of thin unitized components the effects of initial stresses are more relevant and should be considered in formulating mathematical modes. In the studies described in the previous sections it was concluded that

machining-induced stress can lead to structural instability in the absence of external loads, where the bulk or material stresses (present in 7050-T74 and 7050-T7451 aluminum plates) are insufficient to cause pre-load buckling. It is expected however, that the presence of material stresses can affect structural stability to a sufficient degree to cause a significant reduction in the load carrying capacity of a structure.

In this section we investigate the effect of bulk stresses on the buckling strength of a simple test specimen under a constant shearing load, as shown in Figure 12.

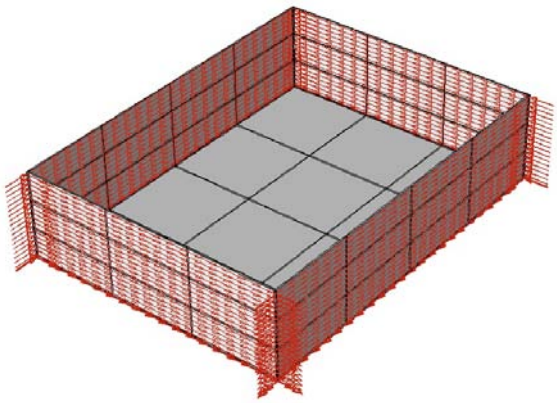

**Figure 12: Box specimen under pure shear.**

The load required to cause the specimen to buckle was computed for three cases:

- Reference case: Box loaded by shear with no residual stresses.
- Box loaded by shear and including the initial bulk stresses of 7050-T74 aluminum plates shown in Figure 3a.
- Box loaded by shear and including the initial bulk stresses of 7050-T7451 aluminum plates shown in Figure 3b.

The computation of the buckling load was performed by an iterative procedure in which the residual stresses were kept constant and the shear load was increased until the buckling load factor was one. The effect of residual stress in the structural stability of the box is represented by the relative difference between the reference solution and the solution including initial stresses. A positive sign means that the residual stresses are increasing the load required to produce structural instability (beneficial effect of residual stresses). On the other hand, a negative sign means that the residual stresses are decreasing the load required to produce structural instability (detrimental effect of residual stresses).

Table 2 shows the computed values for the test specimen. It is observed that the residual stresses affect mainly the buckling load whereas the buckling mode (shown in Figure 13) remains unchanged. The residual stresses present in 7050-T74 aluminum plate, at a location of ex=30.32

mm, increases the stability of the specimen by 38%, while the residual stresses in 7050-T7451 at the same location reduces the buckling strength by 11%.

**Table 2: Shear load required to buckle the specimen, with and without bulk residual stresses (RS).**

| Buckling Shear Load (MPa) | | | |
|---|---|---|---|
| **ex=30.32** | **RS + Load** | **Load alone** | **Stability variation** |
| 7050-T74 | 0.2272 | 0.1645 | 38.12% |
| 7050-T7451 | 0.1463 | 0.1645 | -11.06% |

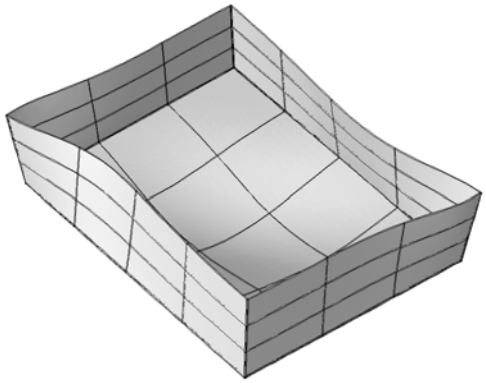

**Figure 13: Buckling mode for box specimen under shear load (with and without bulk residual stresses).**

This investigation indicates that the stability of loaded thin-walled unitized structural components depends not only on the magnitude of the residual stresses but also on the type of loading. If the compressive stresses resulting from external loads combine with the compressive residual stresses, then the effect will be to reduce buckling strength.

It is well known that substantial differences exist between predictions of buckling strength based on mathematical models and the results of physical experiments. These differences are usually attributed to geometric imperfections not incorporated in the model. The results of our investigation indicate that the effects of residual stresses are significant also.

# Delamination of composite materials

The strain energy release rate in damaged laminate composite materials has been identified as the parameter that characterizes the residual strength of unitized structures made of laminate composites [5]. Typical failure in the presence of an initial defect, such as delamination, appears under a mixed mode loading. Therefore is essential to have an efficient algorithm for the computation of the strain energy release rates ($G_i$, $i$=1, 2, 3) associated with each loading mode (opening or tension mode $i$=1, sliding shear mode $i$=2, and scissoring shear mode $i$=3) for the construction a mixed mode failure criterion.

The Virtual Crack Closure Technique (VCCT) is the most commonly used method for the computation of $G_i$. The VCCT is based on the relationship between the energy release rate ($G$) and the work required to return a crack to its original length. This involves the computation of the stresses in the vicinity of the crack tip along a virtual crack extension of size $\Delta a$. Since the stresses at the crack tip are infinity, it is clear that in a numerical approximation this value cannot be achieved (even when the numerical error measured in energy norm can be arbitrarily reduced by using geometric mesh refinement). Furthermore, the singular behavior of the stresses at the crack tip will affect the solution near the crack tip. Therefore the accuracy of the computed value of $G$ will deteriorate when the crack extension $\Delta a$ goes to zero. It follows that the quality of the solution near the crack tip will affect the computed strain energy release; therefore it should not be included in the computation of the energy release rate ($G$).

It was found during our investigation that typical numerical implementations of the VCCT utilizing the h-version of the finite element method (FEM) are inaccurate because the results are mesh-dependent. Typical applications used in the h-version of the finite element method utilize an integral form of the VCCT equations which cancel some of the effects of the singular behavior of the solution at the crack tip. However, the singularity at the crack tip will affect the numerical solution in the vicinity of the crack tip where the computation of the energy release rate becomes mesh dependent.

A modified algorithm using the p-version was developed to overcome this limitation. This algorithm involves the numerical computation of the stresses close to the crack tip, in a region where they can be computed with sufficient accuracy (guaranteed by using a geometric mesh together with a uniform p-extension in order to ascertain the convergence of the solution). This information is used for computing the energy release rate for a reduced crack path [$\varepsilon$, $\Delta a$], where $\varepsilon$ is an arbitrarily small distance measured from the crack tip. Then, since the behavior of the exact solution in the neighborhood of the crack tip is known, the computed solution is used for extrapolating the stress field towards the crack tip on the interval [0, $\varepsilon$] using a closed-form equation, that is used subsequently for obtaining a correction for the computed energy release rate. In this Phase I project we addressed the computation of $G_I$ and $G_{II}$ for two dimensional cases using the p-version of the FEM.

## *The Virtual Crack Closure Technique*

### Formulation

The Virtual Crack Closure Technique (VCCT) is based on the relationship between the energy release rate ($G$) and the work required to return a crack extension to its original length (c.f. [5] and the references therein). A brief description is included in the following.

Consider the state of stresses at the crack tip in an isotropic material for a symmetric (Mode I) loading. For the coordinate system centered on the crack tip, as shown in Fig. 1, and neglecting terms of higher order, the $\sigma_y$ stress distribution along $y$=0 is given by:

$$\sigma_y = \frac{K_I}{\sqrt{2\pi x}} \qquad x \geq 0 \tag{1}$$

The displacement of the (top) crack face is:

$$u_y = \frac{(1+\nu)(\kappa+1)}{E}\frac{K_I}{\sqrt{2\pi}}\sqrt{-x} \qquad x \leq 0 \tag{2}$$

Where $E$ is the modulus of elasticity, $\nu$ is the Poisson's ratio and $\kappa$ is defined as:

$$\kappa = \begin{cases} \dfrac{3-\nu}{1+\nu} & \text{for plane stress} \\ 3 - 4\nu & \text{for plane strain.} \end{cases}$$

Assume now that the crack length increases by a small amount $\Delta a$, as shown in Figure 15. In this case the displacement will be:

$$u_y = \frac{(1+\nu)(\kappa+1)}{E}\frac{K_I}{\sqrt{2\pi}}\sqrt{\Delta a - x} \qquad 0 \leq x \leq \Delta a\ ,\ x' = x - \Delta a$$

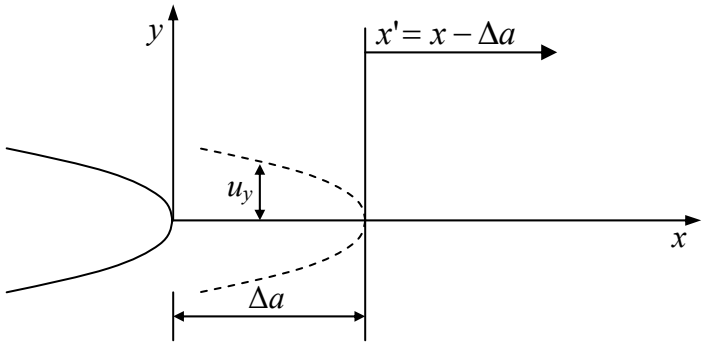


**Figure 15: Crack tip coordinate system. Notation.**

The work required to return the crack to its original length, that is, to close the length increment $\Delta a$, is given by:

$$\Delta W = 2\int_0^{\Delta a}\frac{1}{2}\sigma_y u_y dx = \underbrace{\frac{(1+\nu)(\kappa+1)}{E}\frac{K_I^2}{2\pi}}_{C_1}\underbrace{\int_0^{\Delta a}\sqrt{\frac{\Delta a - x}{x}}dx}_{\Delta a\pi/2} \tag{3}$$

Hence:

$$\Delta W = \frac{(1+\nu)(\kappa+1)}{4E}K_I^2\Delta a$$

In order to restore the crack to its initial length, energy equal to Δ*W* had to be imparted to the elastic body. This is the energy expended in crack growth, called Griffith's surface energy. The potential energy had to decrease by the same amount when the crack increment occurred. Hence:

$$G = -\lim_{\Delta a \to 0} \frac{\Delta \Pi}{\Delta a} = -\frac{\partial \Pi}{\partial a} = \frac{(1+\nu)(\kappa+1)}{4E} K_I^2$$

Therefore the energy release *G* can be computed as:

$$G = -\lim_{\Delta a \to 0} \frac{\Delta W}{\Delta a}$$

When the loading is purely anti-symmetric (Mode II loading), then the relationship between the energy release rate and the work required to return the crack to its original length is analogous to the symmetric case. Instead of equations (1) and (2) we have

$$\tau_{xy} = \frac{K_{II}}{\sqrt{2\pi x}} \qquad x \geq 0 \tag{4}$$

The displacement of the (top) crack face is

$$u_x = \frac{(1+\nu)(\kappa+1)}{E} \frac{K_{II}}{\sqrt{2\pi}} \sqrt{-x} \qquad x \leq 0 \tag{5}$$

In view of the fact that the solutions corresponding to Mode I and Mode II loading are *energy orthogonal*, we have:

$$\Pi(\vec{u}_I + \vec{u}_{II}) = \Pi(\vec{u}_I) + \Pi(\vec{u}_{II}),$$

where $\vec{u}_I$ and $\vec{u}_{II}$ are solutions of the Mode I and Mode II loadings, respectively. Therefore in the case of combined loading we have:

$$G = G_I + G_{II} = \frac{(1+\nu)(\kappa+1)}{4E}(K_I^2 + K_{II}^2).$$

## *Closed-form vs. Numerical approximation of G*

It can be observed from equations (1) and (4) that the stresses at the crack tip are infinity. It is clear that in a numerical approximation requiring the integration of these stresses, even when the numerical error can be arbitrarily reduced by using an appropriated mesh refinement, this infinite value cannot be achieved. Furthermore, the singular behavior of the stresses at the crack tip will affect the numerical solution near the crack tip, and therefore the quality of the computed value for *G* will deteriorate when Δ*a* approaches zero. Because the quality of the solution near the

crack tip will affect the total strain energy release rate, one approach would be to exclude a region near the crack tip from the computation of the energy release rate (*G*). This approach has limitations however.

Consider the error in the computation of the integral expression on equation (3) when excluding a small region of size ε in the neighborhood of the crack tip {*x*| 0 ≤ *x* ≤ *ε*}, that is

$$\Delta W = C_1\left(\int_0^{\varepsilon}\sqrt{\frac{\Delta a - x}{x}}dx + \int_{\varepsilon}^{\Delta a}\sqrt{\frac{\Delta a - x}{x}}dx\right) = C_1\Delta a\frac{\pi}{2} \tag{6}$$

Then we can write:

$$G \cong \frac{\Delta W}{\Delta a} = \frac{C_1}{\Delta a}\left(\int_0^{\varepsilon}\sqrt{\frac{\Delta a - x}{x}}dx + \int_{\varepsilon}^{\Delta a}\sqrt{\frac{\Delta a - x}{x}}dx\right) = C_1\frac{\pi}{2}$$

$$G \cong \frac{\Delta W}{\Delta a} = \frac{C_1}{\Delta a}\int_0^{\varepsilon}\sqrt{\frac{\Delta a - x}{x}}dx + \frac{C_1}{\Delta a}\int_{\varepsilon}^{\Delta a}\sqrt{\frac{\Delta a - x}{x}}dx = C_1\frac{\pi}{2} \tag{7}$$

Now if we compute the second integral in (7) as our approximation for *G*, we have

$$\overline{G} \cong \frac{C_1}{\Delta a}\int_{\varepsilon}^{\Delta a}\sqrt{\frac{\Delta a - x}{x}}dx \tag{8}$$

Where the error will be given by

$$e \cong \frac{C_1}{\Delta a}\int_0^{\varepsilon}\sqrt{\frac{\Delta a - x}{x}}dx \tag{9}$$

And the relative error will be

$$e_r\% = \frac{G - \overline{G}}{G}100\% = \frac{\frac{C_1}{\Delta a}\int_0^{\varepsilon}\sqrt{\frac{\Delta a - x}{x}}dx}{C_1\pi/2} = \frac{2}{\pi\Delta a}\int_0^{\varepsilon}\sqrt{\frac{\Delta a - x}{x}}dx\,100\%$$

Considering the ratio $\varepsilon/\Delta a$ in the interval [0,1] we can compute the relative error associated with the first integral term in equation (7) as shown in Figure 16.

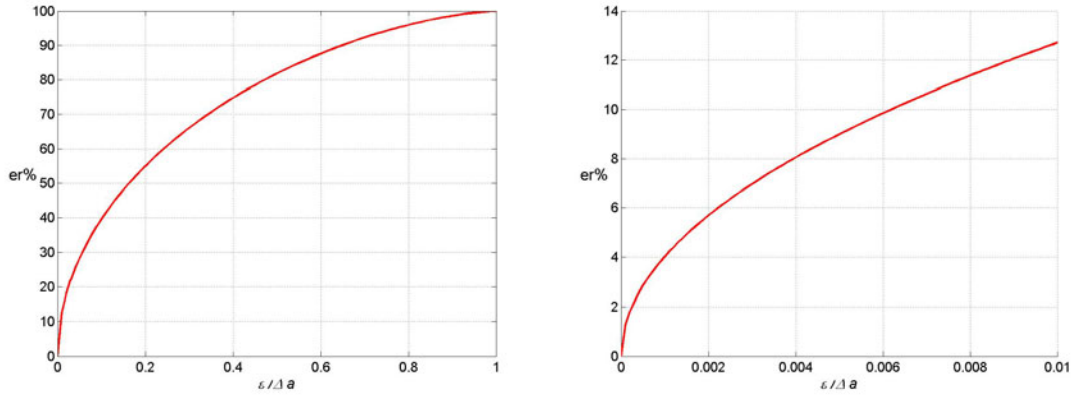


**Figure 16: Relative error associated with the use of equation (8) in the interval [0, 1] (left). Detail in the interval [0, 0.01] (right).**

It can be observed that the contribution of a small region near the crack tip in the computation of the energy release rate (*G*) is of considerable significance. For example, excluding a region of the crack tip of 0.2% the size of the crack increment ($\varepsilon/\Delta a$=0.002), the value of *G* will be off by 6%. It follows that in order to achieve a good approximation of *G*, the stresses near the crack tip have to be known with high accuracy, which is not possible to achieve with the finite element method without the use of highly refined, (geometrically graded) meshes leading to a significant increase in computational cost.

An alternative approach is discussed in the following. The exact solution near the crack tip is of the form $\sigma \approx Ar^{\lambda-1}$, where *A* is a constant and $\lambda$ is the first eigenvalue corresponding to the solution of the corresponding elasticity problem. Therefore, near the crack tip $\sigma_y$ and $\tau_{xy}$ can be approximated as:

$$\sigma_y \approx Ar^{\lambda-1}$$

$$\tau_{xy} \approx Br^{\lambda-1}$$

Then, computing $\sigma_y$ or $\tau_{xy}$ from the finite element solution at two points (Figure 17), it is possible to find *A*, *B,* and $\lambda$ as follows:

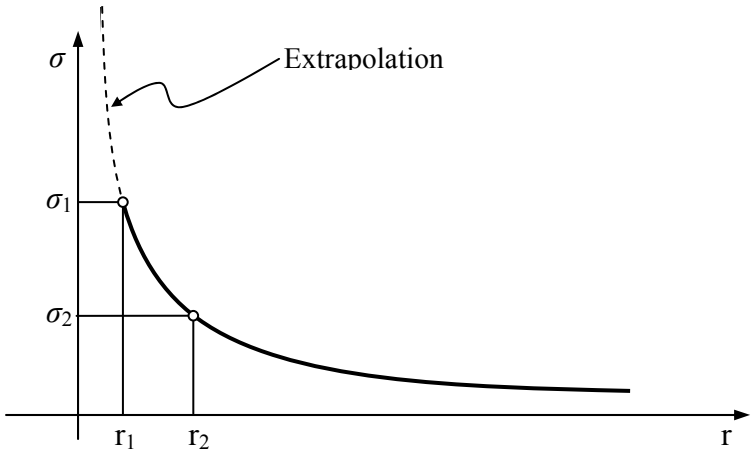


**Figure 17: Approximation of the stress field near the crack tip.**

$$\left.\begin{aligned}\sigma_1 &= A r_1^{\lambda-1}\\ \sigma_2 &= A r_2^{\lambda-1}\end{aligned}\right\} \Rightarrow \begin{cases}\lambda = 1 + \dfrac{\ln \sigma_1 / \sigma_2}{\ln r_1 / r_2}\\ A = \dfrac{\sigma_1}{r_1^{\lambda-1}}\end{cases} \tag{10}$$

Therefore we can estimate the value of *e* in equation (9) by using:

$$\overline{e} \cong \frac{\int_{\varepsilon_o}^{\varepsilon} \sigma_y^{app} u_y^{num} dx}{\Delta a} \tag{11}$$

Where $u_y^{num}$ is obtained from the numerical approximation, and $\sigma_y^{app}$ is computed by evaluating equation (10) at the corresponding points. Since equation (11) has to be computed numerically, we cannot include zero as the lower limit, therefore we use the parameter $\varepsilon_0$ which indicates the first point in the integration interval neglecting the origin. It follows that the quality of the correction will depend on the number of points used for the extraction of $u_y^{num}$.

Finally we compute a corrected value for $\overline{G}$ as:

$$Gc = \overline{G} + \overline{e}$$

This methodology will be illustrated with examples in the following.

## *Example 1* (Mode I loading): Double cantilever beam

The double cantilever beam shown in Figure 18 is made of an isotropic material and loaded in pure Mode I. In this case $G=J$, where $J$ is the J-integral. Therefore we will consider the computed value of $J$ as the reference value[2] for $G$. Material properties: $E$ = 1.010e+007 psi, $v$ = 0.365 (plane stress).

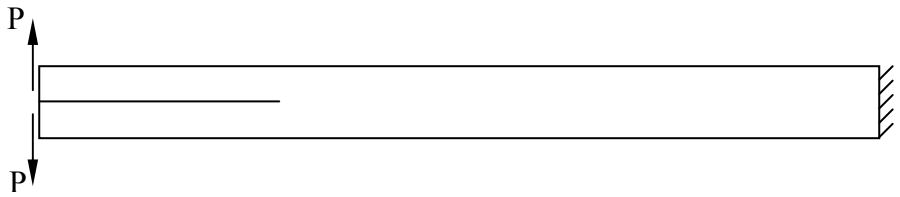


**Figure 18: Double cantilever beam.**

### Mesh

The mesh used for computing the numerical approximations was designed so as to minimize the pollution error caused by the singularity at the crack tip. Five layers of geometrically graded elements towards the crack tip where used as shown in Figure 19. Because of symmetry, only one half of the beam was considered for the analysis.

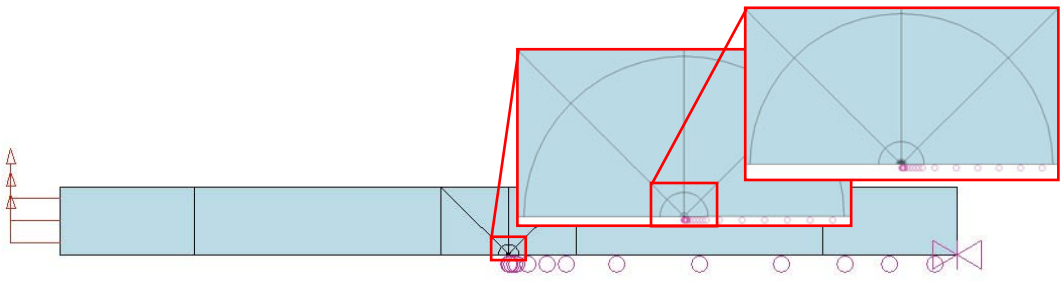

**Figure 19: Mesh and boundary conditions for example 1.**

### Extraction

For each interval $\Delta a$ the approximated value of the energy release rate ($\overline{G}$) was computed numerically using expression (12), and analytically, using expression (8).

[2] The J-integral is computed using the finite element software StressCheck.

$$\overline{G}_I = \frac{\int_{\varepsilon}^{\Delta a} \sigma_y^{num} u_y^{num} dx}{\Delta a} \tag{12}$$

**Reference value (*J*):** The finite element solution was obtained by p-extension using the mesh shown in Figure 19. The polynomial order of the elements was increased from 1 to 8 and the fracture mechanics parameters (KI, KII and J) were extracted for each one of the eight solutions and the results shown in Table 3 as a function of the number of degrees of freedom (DOF). It can be seen that the value of *J* remains practically unchanged for the last three solutions. The value *J*=0.034592 was used as the reference solution for *G*.

**Table 3: Computed values of $K_I$, $K_{II}$ and *J*.**

| DOF | KI | KII | J |
|---|---|---|---|
| 68 | 507.24 | 0 | 1.0665e-02 |
| 192 | 646.05 | 0 | 2.8653e-02 |
| 324 | 586.50 | 0 | 3.1507e-02 |
| 512 | 585.97 | 0 | 3.3492e-02 |
| 756 | 591.85 | 0 | 3.4389e-02 |
| 1056 | 591.23 | 0 | 3.4585e-02 |
| 1412 | 590.63 | 0 | 3.4606e-02 |
| 1824 | 590.80 | 0 | 3.4592e-02 |

**Energy release rate (*G*):** The computation of the approximated energy release rate $\overline{G}$ was performed using equation (12) for three values of $\Delta a$, with the values of the stress ($\sigma_y$) and displacement ($u_y$) obtained from the finite element solution corresponding to 1824 DOF. The results are shown in Table 4. The percent relative error was computed as: $e_r = \frac{J - \overline{G}}{J} \times 100$

**Table 4: Computed values of $\overline{G}$ and the relative error (%) with respect to *J*.**

| $\Delta a$ | $\varepsilon$ | $\overline{G}$ | $e_r$% |
|---|---|---|---|
| 8.1818e-03 | 3.0375e-04 | 2.5994e-02 | 24.8 % |
| 1.6363e-02 | 3.0375e-04 | 2.8383e-02 | 17.9 % |
| 2.4545e-02 | 3.0375e-04 | 2.9429e-02 | 14.9 % |

The computation of the correction for the approximated energy release rate was performed by extracting $u_y^{num}$ at 100 (equidistant) points, and 500 (equidistant) points in the interval [0, $\varepsilon$]. The effect of the addition of the correction term in the value of $\overline{G}$ is shown in Figure 20 as a function of $\Delta a$. The reference solution is independent of $\Delta a$, and the other three solutions shown in the

figure are for the cases of no correction ($G_0$), and with corrections for 100 ($G_{100}$) and 500 ($G_{500}$) extraction points. The relative error for each case is shown in Figure 21. The number of points to extract $u_y^{num}$ determines the value for $\varepsilon_0$ that is going to limit the quality of the approximation. The results obtained for 100 and 500 points are shown in Tables 5 and 6.

**Table 5: Corrected values of $\overline{G}$ and its relative error with respect to *J* for 100 points.**

| **Δa** | **$\varepsilon_0$** | **Gc** | **$e_r$%** |
|---|---|---|---|
| 8.1818e-03 | 3.01e-06 | 3.3738e-02 | 2.47 % |
| 1.6363e-02 | 3.01e-06 | 3.3983e-02 | 1.76 % |
| 2.4545e-02 | 3.01e-06 | 3.4094e-02 | 1.44 % |

**Table 6: Corrected values of $\overline{G}$ and its relative error with respect to *J* for 500 points.**

| **Δa** | **$\varepsilon_0$** | **Gc** | **$e_r$%** |
|---|---|---|---|
| 8.1818e-03 | 6.1e-07 | 3.4206e-02 | 1.11 % |
| 1.6363e-02 | 6.1e-07 | 3.4323e-02 | 0. 78 % |
| 2.4545e-02 | 6.1e-07 | 3.4378e-02 | 0. 62 % |

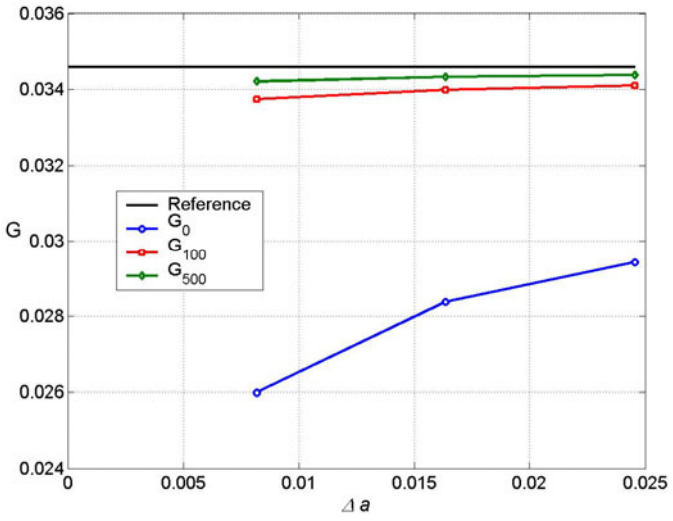


**Figure 20: Computed value of $\overline{G}$ ($G_0$) and its corrections for 100 ($G_{100}$) and 500 ($G_{500}$) points extraction.**

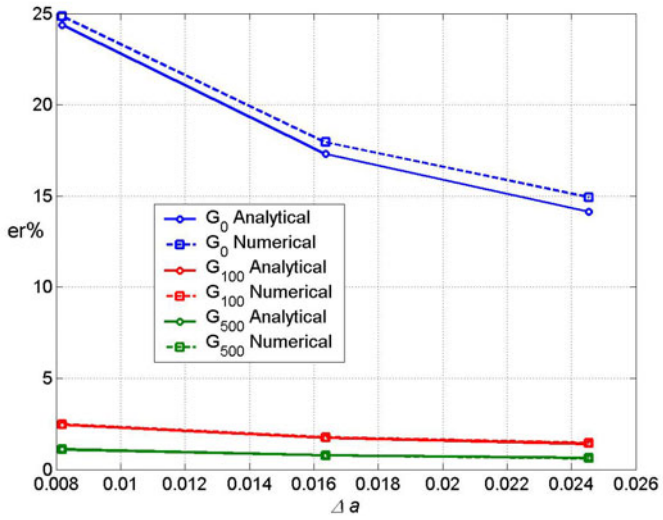


**Figure 21: Computed numerical and analytical error for $\overline{G}$ ($G_0$) and its corrections for 100 ($G_{100}$) and 500 ($G_{500}$) points extraction.**

**Correction using and extrapolation function for σ and *u*:** The results shown in Tables 5 and 6 indicate that the solution still depends on the value of $\varepsilon_0$ since the numerical integral for the correction term must exclude the origin. An alternative approach was considered to remove this limitation. The problem in using equation (11) is that the integral has to be performed numerically because the displacement is known from the numerical solution, and that precludes extending the integration limit to include zero. The solution is to perform the integral analytically which requires an approximation of the displacement function in the integration interval. Near the crack tip the displacement $u_y$ is of the form $u_y \cong Br^{\lambda}$. Therefore it is possible to write an approximation for $u_y$ as:

$$\left.\begin{aligned} u_{y_1} &= Br_1^{\lambda} \\ u_{y_2} &= Br_2^{\lambda} \end{aligned}\right\} \Rightarrow \begin{cases} \lambda = \dfrac{\ln u_{y_1}/u_{y_2}}{\ln r_1/r_2} \\ B = \dfrac{u_{y_1}}{r_1^{\lambda}} \end{cases}$$

where 1 and 2 refer to two points along the crack tip coordinate system as shown in Figure 17. The correction for the energy density function ($G$) using[3]:

[3] The reason for using $\lambda_1$ and $\lambda_2$, instead of a single value $\lambda$ is because these values are computed from fitting numerical data, and therefore they are expected to be slightly different, whereas in theory they should be the same.

$$\bar{e} \cong \frac{\int_0^{\varepsilon} \sigma_y^{app} u_y^{app} dx}{\Delta a} = \frac{AB\int_0^{\varepsilon} x^{\lambda_1 - 1}(\Delta a - x)^{\lambda_2} dx}{\Delta a}$$

With A given in equation (10). This integral can be written as:

$$\bar{e} = AB\frac{\Delta a^{\lambda_2 - 1}\varepsilon^{\lambda_1}}{\lambda_1}\sum_{k=0}^{\infty}\frac{(\lambda_1)_k(-\lambda_2)_k}{(1+\lambda_1)_k}\frac{\varepsilon^k}{k!}$$

Where any term between brackets, such as $(\lambda_1)_k$, is expanded as $(\lambda_1)_k = \lambda_1(\lambda_1+1)\cdots(\lambda_1+k-1)$. We refer to Mathematica.[4] We observe that the solution for this integral exist and is bounded, however we need to compute a series expansion in order to obtain an approximated value. Alternatively, since the function $u_y$ is not extracted at the crack tip but at the end of the crack increment $\Delta a$ were the function $u$ is very smooth, we can approximate $u_y$ by a linear function, that is $u_y = Bx+C$. Then,

$$B = \frac{u_{y_2} - u_{y_1}}{x_2 - x_1},\ C = u_{y_1} - Bx_1$$

It follows that

$$\bar{e} \cong \frac{\int_0^{\varepsilon} \sigma_y^{app} u_y^{app} dx}{\Delta a} = \frac{\int_0^{\varepsilon} Ax^{\lambda-1}\left[B(\Delta a - x) + C\right]dx}{\Delta a}$$

$$= \frac{A}{\Delta a}\left[-B\int_0^{\varepsilon} x^{\lambda} dx + \left(C + B\Delta a\right)\int_0^{\varepsilon} x^{\lambda-1} dx\right]$$

$$= \frac{A}{\Delta a}\left[-B\frac{\varepsilon^{\lambda+1}}{\lambda+1} + \left(C + B\Delta a\right)\frac{\varepsilon^{\lambda}}{\lambda}\right] \tag{13}$$

The case for mode II loading is analogous. The results shown in Table 7 were obtained using equation (13) to compute the correction for $\bar{G}$.

[4] Mathematica is a trademark of Wolfram Research, Inc.

**Table 7: Values of Gc and its relative error with respect to *J* using an approximated closed form for the correction term.**

| *Δa* | *J* | *Gc* | *er%* |
|---|---|---|---|
| 8.1818e-03 | 3.4592e-02 | 3.4596e-02 | 0.0125 % |
| 1.6363e-02 | 3.4592e-02 | 3.4605e-02 | 0.0388 % |
| 2.4545e-02 | 3.4592e-02 | 3.4616e-02 | 0.0681 % |

## *Example 2* (Mode II loading): Plate with a crack under pure shear.

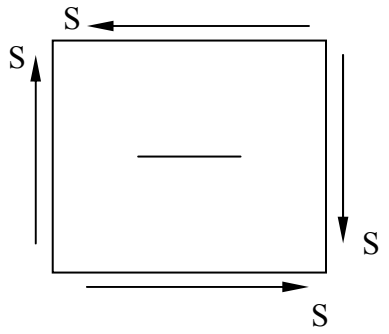


**Figure 24: Plate with a crack under pure shear.**

The problem shown in Figure 24 corresponds to a flat panel of constant thickness with a central crack under pure shear. Isotropic material properties are considered in order to provide a reference solution. Since this case is in pure Mode II the value of the energy release rate ($G_{II}$) will be coincident with the value of the J integral ($J$). Therefore we will consider the computed value of $J$ as the reference value for $G_{II}$. Material properties: $E$ = 1.010e+007 psi, $v$ = 0.365 (plane stress).

**Mesh**

The mesh used for computing the numerical approximations was designed so as to minimize the pollution error caused by the singularity at the crack tip. Four geometrically graded layers of elements where used with such purpose as shown in Figure 25. Because of symmetry, one quarter of the plate was considered for the analysis.

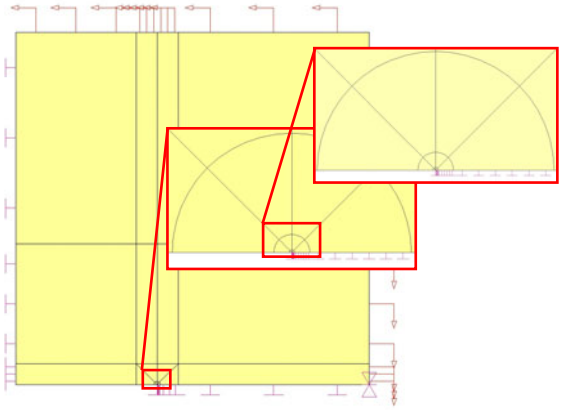

**Figure 25: Mesh and boundary conditions for example 2.**

### Extraction

For each interval $\Delta a$ the approximated value ($\overline{G}$) of the energy release rate ($G$) was computed both numerically, using expression (14), and analytically, using expression (8).

$$\overline{G}_{II} = \frac{\int_{\varepsilon}^{\Delta a} \tau_{xy}^{num} u_x^{num} dx}{\Delta a} \tag{14}$$

**Reference value ($J$):** The reference solution was obtained by p-extension using the finite element mesh shown in Figure 25. The polynomial order of the elements was increased from 1 to 8 and the fracture mechanics parameters were extracted for each one of the eight solutions and the results shown in Table 8 as a function of the number of degrees of freedom (DOF). It can be seen that the value of $J$ remains practically unchanged for the last three solutions. The value $J$=0.39661 was used as the reference solution.

**Table 8: Computed values of $K_I$, $K_{II}$ and $J$.**

| DOF | KI | KII | J |
|---|---|---|---|
| 59 | 0 | -1428.7 | 1.8779e-01 |
| 171 | 0 | -1913.3 | 3.3865e-01 |
| 291 | 0 | -2031.0 | 3.9681e-01 |
| 463 | 0 | -2014.6 | 4.0095e-01 |
| 687 | 0 | -2001.5 | 3.9911e-01 |
| 963 | 0 | -1998.2 | 3.9723e-01 |
| 1291 | 0 | -1999.6 | 3.9655e-01 |
| 1671 | 0 | -2001.5 | 3.9661e-01 |

**Energy release rate (*G*):** The computation of the approximated energy release rate $\overline{G}$ was done using equation (14) for three values of Δ*a,* with the values of the stress ($\tau_{xy}$) and displacement ($u_x$) obtained from the finite element solution corresponding to 1671 DOF. The results are shown in Table 9.

**Table 9: Computed values of $\overline{G}$ and its relative error with respect to *J*.**

| Δ*a* | $\varepsilon$ | $\overline{G}$ | *er%* |
|---|---|---|---|
| 2.25e-03 | 5.0625e-04 | 1.6645e-01 | 58.12 % |
| 4.50e-03 | 5.0625e-04 | 2.3068e-01 | 41.96 % |
| 6.75e-03 | 5.0625e-04 | 2.6037e-01 | 34.49 % |

The computation of the correction for the approximated energy release rate was performed using expression analogous to equation (13), and the results are shown in Table 10.

**Table 10: Corrected values of $\overline{G}$ and its relative error with respect to *J* using an approximated closed form for *e*.**

| Δ*a* | *J* | *Gc* | *er% (comd)* |
|---|---|---|---|
| 2.25e-03 | 3.9661e-01 | 3.9906e-01 | 0.402 % |
| 4.50e-03 | 3.9661e-01 | 3.9704e-01 | 0.107 % |
| 6.75e-03 | 3.9661e-01 | 3.9682e-01 | 0.161 % |

## *Example 3* (Mode I loading)

Consider the same model problem of example 1 (Figure 18) using orthotropic materials properties ($E_{LL}$ = 8.0e6 psi, $E_{TT}$ = 1.0e6 psi, $v_{LT}$ = 0.3, $G_{LT}$ = 0.6e6 psi, plane stress). Since there is material, geometric and load symmetry the problem remains a pure Mode I loading and mesh shown in Figure 19 was used for the analysis. Therefore we can use *J* as the reference value for $G_I$.

**Reference value (*J*):** The reference solution was obtained by p-extension and the results shown in Table 11. The value *J*=0.052817 was used as the reference solution.

**Table 11: Computed values of *J*.**

| DOF | J |
|---|---|
| 68 | 2.7688e-02 |
| 192 | 4.6019e-02 |
| 324 | 4.9508e-02 |
| 512 | 5.2128e-02 |
| 756 | 5.2759e-02 |
| 1056 | 5.2845e-02 |
| 1412 | 5.2843e-02 |
| 1824 | 5.2817e-02 |

**Energy release rate (*G*):** The computation of the approximated energy release rate $\overline{G}$ was done using equation (12) with the values of the stress ($\sigma_y$) and displacement ($u_y$) obtained from the finite element solution corresponding to 1824 DOF. The results are shown in Table 12.

**Table 12: Computed values of $\overline{G}$ and its relative error with respect to *J*.**

| **Δ*a*** | ***ε*** | $\overline{G}$ | ***er%*** |
|---|---|---|---|
| 8.1819e-03 | 3.038e-04 | 3.9780e-02 | 24.65 % |
| 1.6364e-02 | 3.038e-04 | 4.3478e-02 | 17.68 % |
| 2.4545e-02 | 3.038e-04 | 4.5102e-02 | 14.61 % |

Using equation (13) to compute the correction for $\overline{G}$, the results shown in Table 13 were obtained, providing a clear indication that the benefits of the approach in the computation of the energy release rate demonstrated for isotropic materials is also realized for orthotropic materials.

**Table 13: Values of $\overline{G}$ and its relative error with respect to *J* using an approximated closed form for the correction term.**

| **Δ*a*** | ***J*** | ***Gc*** | ***er%*** |
|---|---|---|---|
| 8.1819e-03 | 5.2817e-02 | 5.2817e-02 | 1.41e-04 % |
| 1.6364e-02 | 5.2817e-02 | 5.2816e-02 | 1.08e-03 % |
| 2.4545e-02 | 5.2817e-02 | 5.2821e-02 | 6.61e-03 % |

## *Example 4* (Mode II loading)

Consider once again the model problem of example 2 (Figure 24) however this time using orthotropic materials properties

($E_{LL}$ = 8.0e6 psi, $E_{TT}$ = 1.0e6 psi, $v_{LT}$ = 0.3, $G_{LT}$ = 0.6e6 psi, plane stress). Since there is material, geometric symmetry and load anti-symmetry, the plate is under pure Mode II loading when using an orthotropic material aligned with the geometric axis. Therefore we can use *J* as the reference value for $G_{II}$.

**Reference value (*J*):** The reference solution was obtained by p-extension and the results shown in Table 14. The value *J*=1.0315 was used as the reference solution.

**Table 14: Computed values of *J*.**

| DOF | J |
|---|---|
| 68 | 2.5843e-02 |
| 197 | 6.5063e-01 |
| 334 | 8.2705e-01 |
| 531 | 9.3559e-01 |
| 788 | 9.9751e-01 |
| 1105 | 1.0204e+00 |
| 1482 | 1.0287e+00 |
| 1919 | 1.0315e+00 |

**Energy release rate (*G*):** Computation of the approximated energy release rate $\overline{G}$ was done as described before and the results are shown in Table 15.

**Table 15: Computed values of $\overline{G}$ and its relative error with respect to *J*.**

| Δ*a* | *ε* | $\overline{G}$ | *er%* |
|---|---|---|---|
| 2.25e-03 | 5.0625e-04 | 4.3204e-01 | 58.12 % |
| 4.50e-03 | 5.0625e-04 | 5.9989e-01 | 41.84 % |
| 6.75e-03 | 5.0625e-04 | 6.7736e-01 | 34.33 % |

Using equation (12) to compute the correction for $\overline{G}$ in, we obtained the results shown in Table 16. Note that for this case the error was still under 1% but larger than for the other model problems.

**Table 16: Values of $\overline{G}$ and its relative error with respect to *J* using an approximated closed form for the correction term.**

| Δ*a* | *J* | *Gc* | *er%* |
|---|---|---|---|
| 2.25e-03 | 1.0315e+00 | 1.0254e+00 | 0.59 % |
| 4.50e-03 | 1.0315e+00 | 1.0247e+00 | 0.66 % |
| 6.75e-03 | 1.0315e+00 | 1.0261e+00 | 0.53 % |

## *Example 5* (Mixed mode): Plate with a crack under shear and axial tension.

In order to provide a case of study for a mixed mode loading, and at the same time have enough information to correlate results with other solution techniques, the problem shown in Figure 27 was considered, representing a flat panel of constant thickness with a central crack subjected to the combined effects of shear and tension loads. The material properties are the same as those used for problems 3 and 4.

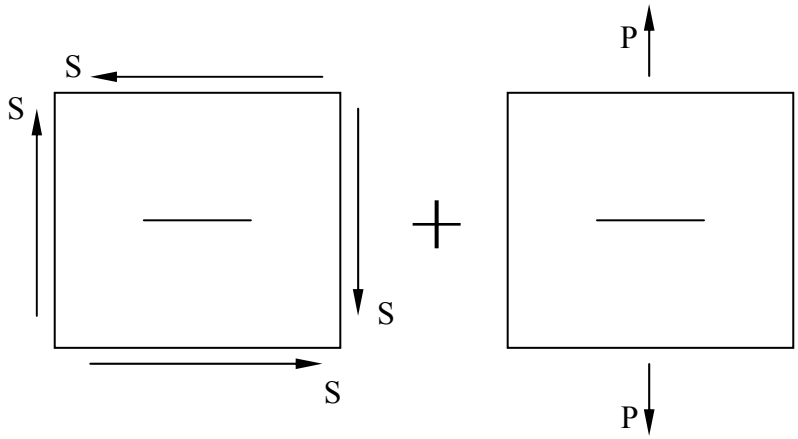


**Figure 27: Proposed model for mixed mode.**

Since in this example $G_{II}$ has to be equal than the one computed for *Example 4*, and $G_T = G_I + G_{II} = J$, we can use this values as a reference to determine the accuracy of the method under a mixed mode.

**Mesh**

The mesh used for computing the numerical approximations was designed so as to minimize the pollution error caused by the singularity at the crack tip. Four geometrically graded layers of elements where used with such purpose as shown in Figure 28.

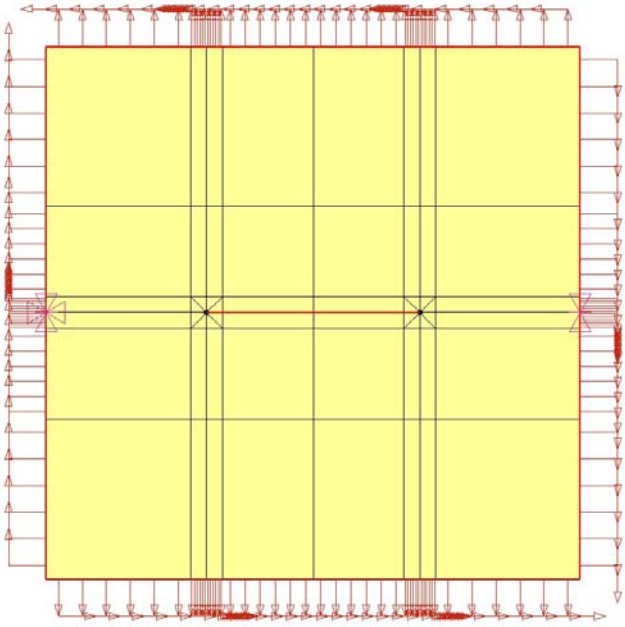

**Figure 28: Mesh and boundary conditions for example 5.**

**Reference value (*J*):** The reference solution was obtained by p-extension using the finite element mesh shown in Figure 28. The polynomial order of the elements was increased from 1 to 8 and the J-integral was extracted for each one of the eight solutions and the results shown in Table 17 as a function of the number of degrees of freedom (DOF). It can be seen that the value of *J* remains practically unchanged for the last three solutions. The value *J*=3.9865 was used as the reference solution.

**Table 17: Computed values of *J*.**

| DOF | J |
|---|---|
| 255 | 2.6171e+00 |
| 737 | 3.1841e+00 |
| 1251 | 3.5666e+00 |
| 1989 | 3.7891e+00 |
| 2951 | 3.9091e+00 |
| 4137 | 3.9606e+00 |
| 5547 | 3.9800e+00 |
| 7181 | 3.9865e+00 |

**Reference value ($G_{II}$):** Assuming superposition, the reference solution for the energy release rate corresponding to the second (shearing) mode $G_{II}$ is provided by the energy release rate computed in Example 4, while the value of *J* can be compared with the sum of $G_I + G_{II}$. Table 18 shows the results of the computation of the approximated energy release rate $\overline{G}$ utilizing equations (12) and (14).

**Table 18: Computed values of $\overline{G}_I$, $\overline{G}_{II}$, $\overline{G}_T = \overline{G}_I + \overline{G}_{II}$ and its relative error with respect to *J*.**

| Δ*a* | *ε* | $\overline{G}_I$ | $\overline{G}_{II}$ | $\overline{G}_T$ | *J* | *er%* |
|---|---|---|---|---|---|---|
| 2.25e-03 | 5.0625e-04 | 1.2378 | 4.3241e-01 | 1.6702 | 3.9865 | 58.10 % |
| 4.50e-03 | 5.0625e-04 | 1.7246 | 5.9189e-01 | 2.3165 | 3.9865 | 41.89 % |
| 6.75e-03 | 5.0625e-04 | 1.9526 | 6.6254e-01 | 2.6151 | 3.9865 | 34.40 % |

Using equation (13) to compute the correction for $\overline{G}_I$ and $\overline{G}_{II}$, the results shown in Tables 19 and 20 were obtained.

**Table 19: Corrected values of $\overline{G}_I$, $\overline{G}_{II}$, $\overline{G}_T$ and its relative error with respect to *J* using an approximated closed form for the correction term.**

| Δ*a* | $G_Ic$ | $G_{II}c$ | $G_Tc$ | *J* | *er%* |
|---|---|---|---|---|---|
| 2.25e-03 | 2.9561 | 1.0157 | 3.9718 | 3.9865 | 0.37 % |
| 4.50e-03 | 2.9650 | 1.0033 | 3.9683 | 3.9865 | 0.46 % |
| 6.75e-03 | 2.9739 | 9.97e-01 | 3.9710 | 3.9865 | 0.39 % |

**Table 20: Corrected values of $\overline{G}_{II}$ and its relative error with respect to $Jref$ obtained in *Example 4*.**

| **Δa** | **$G_{II}c$** | $Jref$ | **er%** |
|---|---|---|---|
| 2.25e-03 | 1.0157 | 1.0315 | 1.54 % |
| 4.50e-03 | 1.0033 | 1.0315 | 2.73 % |
| 6.75e-03 | 9.97e-01 | 1.0315 | 3.45 % |

It is observed that the computation of $G_I$ and $G_{II}$ for a mixed mode loading provides results with acceptable error bounds. The method is considered to be adequate for the computation of $G_I$ and $G_{II}$ for composite materials in 2D. The extension of the proposed methodology for the computation of the energy release rate components in three-dimensions will be included in the proposal for the Phase II project.

# Summary and Conclusions

One of the main goals of this project was the investigation of mathematical models for the simulation of structural stability and post-buckling responses of light-weight unitized airframe components fabricated from aluminum plates by high speed machining techniques. It has been observed in machining experiments that some thin-walled components exhibit local buckling even in the unloaded condition, due to residual stresses. Therefore the effects of residual stresses were taken into account in simulations performed for the purposes of computing the buckling behavior with and without external loads.

The effect of residual stresses on the structural stability of thin unitized components machined from aluminum plates, in particular 7050-T74 and 7050-T7451 plates, was investigated. The findings indicated that residual stresses induced in the plate during the rolling operation (bulk stresses) and residual stresses caused by high speed machining (machining-induced residual stresses) have a significant effect on the stability and should be included as part of the modeling assumption when designing thin unitized components. It was also found that bulk residual stresses are not large enough to cause the specimen to buckle after removing the machined part from the fixture, but they may have a detrimental effect on the buckling load once the component is loaded. Machining-induced residual stresses on the other hand are capable of producing buckling once the part is removed from the fixture.

The second goal was to develop a procedure to determine the residual strength of structures made of composite materials damaged by delamination. To that goal, the implementation of a modified virtual crack closure technique for the computation of the energy release rate in two dimensions was investigated. The advantages of the algorithm was demonstrated by solving model problems in Mode I, Mode II and mixed mode loading for isotropic and orthotropic materials.

# Future work

## *Residual stresses and structural stability*

The preliminary procedure developed to incorporate the effects of residual stresses, either material (bulk) or machining-induced, in the onset of stability of unitized components was demonstrated to be highly effective. However, the procedure is very time-consuming and needs to be optimized and automated. There are also some limitations on the current implementation that need to be removed. Since the residual stresses are introduced by means of a thermal load, the application of external loads is restricted to loads that satisfy the equilibrium condition, since additional constraints can affect the desired residual stress distribution. These activities will be incorporated as part of the Phase II proposal.

## *Delamination of composite materials*

The modified virtual crack closure technique investigated during the Phase I project provides an effective and reliable procedure for the computation of the strain energy release rates for mixed modes in orthotropic materials. Research that will address implementation of the methodology within the framework of StressCheck and its extension to three-dimensional analysis will be one of the main objectives of the Phase II project.

# References

[1] M. Prime. *Residual stress, Stress Relief, and Inhomogeneity in Aluminum Plate*. Scripta Materialia, 2002, Vol 46, Nro 1, pp 77-82.

[2] S. Nervi. *A mathematical Model for the Estimation of the Effects of Residual Stresses in Aluminum Plates*. DSc. Dissertation. Washington University in St. Louis, 2005.

[3] K. Young. *Machining-Induced Residual Stresses and Distortion of Thin Parts*. DSc. Dissertation. Washington University in St. Louis, 2005.

[4 K. Young, S. Nervi and B. A. Szabó. *Machining-Induced Residual Stresses and Distortion*. SAE Paper 05-AMT-75.

[5] R. Krueger, *The Virtual Crack Closure Technique: History, Approach and Applications.* ICASE Report No. 2002-10. NASA/CR-2002-211628, April 2002.

[6] E. F. Rybicki and M. F. Kanninen. *A Finite Element Calculation of Stress Intensity Factors by a Modified Crack Closure Integral*. Engineering Fracture Mechanics, 1977, Vol 9, pp 931-938.

[7] R. Krueger, P. J. Minguet, and T. K. O'Brien. *Implementation of Interlaminar Fracture Mechanics in Design: An Overview*. 14th International Conference on Composite Materials (ICCM-14), San Diego, July 14-18, 2003.

[8] B. Szabo and I. Babuska. *Finite Element Analysis*. Jhon Wiley & sons Inc., 1991.